Dissipative Soliton Resonance in a Wavelength-Tunable Thulium-Doped Fiber Laser With Net-Normal Dispersion
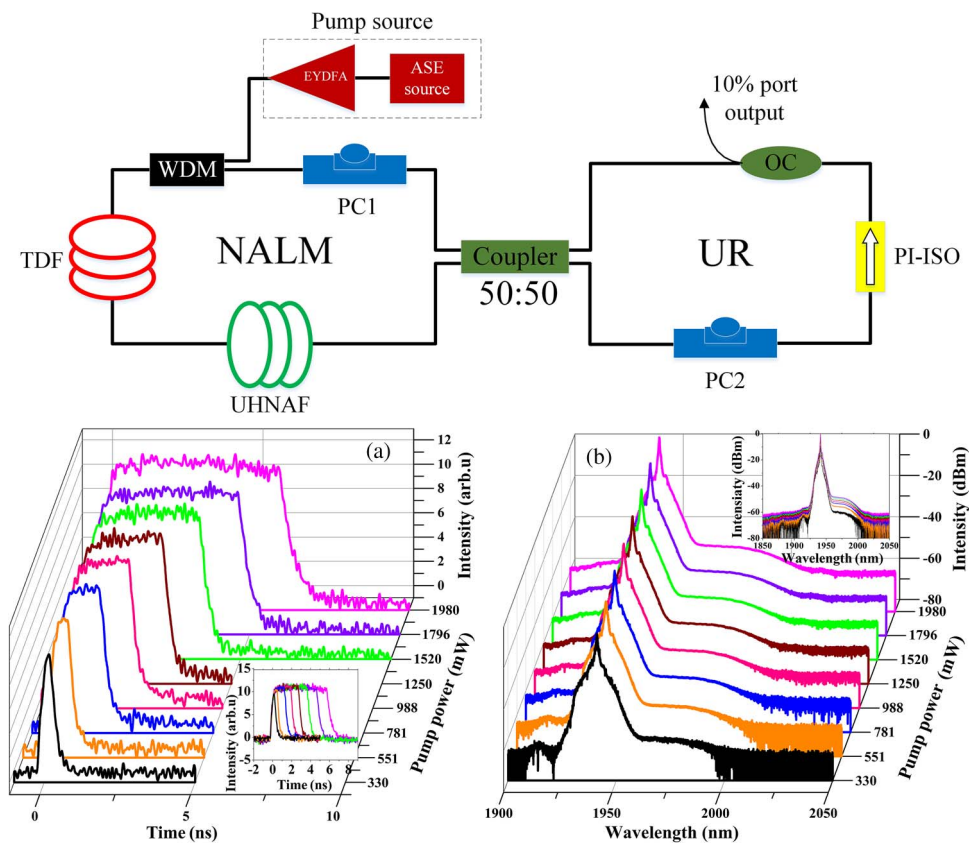
Yi Xu
Yu-li Song
Ge-guo Du
Pei-guang Yan
Chun-yu Guo
Guo-liang Zheng
Shuang-chen Ruan

Dissipative Soliton Resonance in a Wavelength-Tunable Thulium-Doped Fiber Laser With Net-Normal Dispersion

Yi Xu,[1,2,3] Yu-li Song,[1,2,3] Ge-guo Du,[1,2,3] Pei-guang Yan,[2,3,4] Chun-yu Guo,[2,3,4] Guo-liang Zheng,[1] and Shuang-chen Ruan[2,3,4]

[1]College of Electronic Science and Technology, Shenzhen University, Guangdong 518060, China
[2]Shenzhen Key Laboratory of Laser Engineering, Shenzhen 518060, China
[3]Key Laboratory of Advanced Optical Precision Manufacturing Technology of Guangdong Higher Education Institutes, Shenzhen University, Shenzhen 518060, China
[4]College of Optoelectronic Engineering, Shenzhen University, Shenzhen 518060, China

Abstract: We demonstrate an all-fiber figure-eight mode-locked thulium-doped fiber laser with a wide tunable range in both pulsewidth and wavelength. A 45-m-long ultra-high numerical aperture fiber is used to manage the cavity dispersion, and the net cavity dispersion is calculated to be 0.8585 ps^2 at 1900 nm. With net-normal dispersion, the experimental laser, operating in a dissipative soliton resonance region, generates stable rectangular pulses. The pulsewidth varies from 480 ps to 6.19 ns with the increasing pump power, and its center wavelength has a 28.95-nm tunable range (from 1940.22 to 1969.17 nm) by properly adjusting the polarization controllers. The maximum of average output power and pulse energy is 60.73 mW and 19.51 nJ, respectively. The rectangular pulses have a clamped peak power of about 3.16 W. The wavelength-tunable fiber laser with high-energy output operating at 2 μm has great potential in various application fields.

Index Terms: Fiber lasers, mode-locked lasers, tunable lasers, solitons.

1. Introduction

Mode-locked Thulium-doped fiber lasers (TDFLs) operating in an eye-safe spectral region of 2-μm have attracted extensive attention due to their plenty of potential applications in remote sensing, mid-infrared spectrum generation or supercontinuum generation, free-space communication, medicine, metrology, and material processing. Passively mode-locking technology is considered as a useful tool to produce ultrashort pulse. Basically, a passively mode-locked fiber laser employs a nonlinear element, a device with an intensity-dependent response that allow for the formation of optical pulse other than continuous-wave lasing. This device is usually called saturable absorber (SA), such as semiconductor saturable absorber mirror (SESAM) [1]. Many materials developed recently can be used as a good SA as well, including carbon nanotubes (CNTs) [2], graphene [3]–[5], WS$_2$ [6], few-layered MoS$_2$ [7]–[9], and topological insulators (TIs) such as Bi$_2$Se$_3$ [10]–[12] and Bi$_2$Te$_3$ [13]–[15]. In addition, an effective SA based on the

nonlinear phase shift, which is induced by self-phase modulation (SPM) and cross-phase modulation (XPM), is another way to generate mode-locked pulses, such as nonlinear polarization evolution (NPE) [16] and nonlinear amplifying loop mirror (NALM) [17]. Both NPE and NALM provide efficient self-switching, pedestal suppression, and pulse shaping that are equivalent to a real saturable absorber.

Dissipative soliton resonance (DSR), which is a phenomenon that exists in a dissipative system with narrow cavity parameter space, has attracted much attention in the past decade. Governed by the cubic–quintic Ginzburg–Landau equation (CGLE), lasers operating in DSR region have many unique properties such as wide pulse duration, giant chirp, low pulse peak power and large pulse energy. When the cavity parameters match the DSR condition, laser turns to operate in DSR region and generates high-energy rectangular pulses without wave-breaking. With the increasing pump power, the width of DSR pulses monotonously increases and the pulse energy can be infinitely high [33]. The DSR phenomenon has been investigated in both normal and abnormal dispersion regimes, theoretically [18]–[21], [33], and experimentally [22]–[28].

However, most of the previous researches are focused on Ytterbium-doped fiber laser (YDFL) and Erbium-doped fiber laser (EDFL) operating at 1-μm and 1.5-μm, respectively. Recently, dispersion-managed soliton (DS) investigations based on TDFL are growing vigorously. In 2011, Gumenyuk et al. firstly reported a dissipative dispersive managed soliton fiber laser operating at 2 μm. They used SESAM as the SA to obtain mode-locked pulses and chirp fiber Bragg grating (CFBG) to compensate dispersion. By changing the length of passive fiber, the comparison of laser properties in different cavity dispersion has been presented [29]. In 2012, Haxsen *et al.* reported on a TDFL hybrid mode-locked by NPE technique and SESAM. The cavity dispersion is managed by a small-core, high-NA fiber which provides normal dispersion in the 2-μm wavelength region. They obtained mode-locked pulses with 0.7 nJ energy at a center wavelength of 1927 nm and 482 fs duration [30]. The same year, by using NPE technique, Wienke *et al.* reported on an ultrafast TDFL with a fiber-based dispersion management. The TDFL delivered pulses with 170 pJ energy and 119 fs duration [31].

In our experiment, we demonstrate the DSR phenomenon of an all-fiber figure-eight TDFL with dispersion compensated by the ultra-high numerical aperture fiber (UHNAF). The net cavity dispersion is about 0.8585 ps^2 at 1900 nm. By using the NALM technique, stable mode-locked pulses with a repetition rate of 3.11 MHz are obtained. The rectangular pulse width can be tuned from 480 ps to 6.19 ns by increasing the pump power. At the pump power of 1980 mW, the maximum average output power is 60.73 mW, and the pulse energy is as high as 19.51 nJ. Due to the linear increase of pulse energy and pulse width, the peak power are clamped at about 3.16 W. Moreover, by properly adjusting the PCs, we find that the lasing wavelength can be tuned from 1940.22 nm to 1969.17 nm. The wavelength-tuning range is about 28.95 nm. To the best of our knowledge, this is the first demonstration of rectangular pulses generation in an all-fiber figure-eight TDFL operating in the DSR region.

2. Experimental Setup

The schematic of the all-fiber figure-eight TDFL is shown in Fig. 1. The left part is a nonlinear amplified loop mirror (NALM), and the right part is a unidirectional ring (UR). A 2 × 2 3 dB fused fiber coupler is used to connect the two parts. The pump source, with the maximum output power of 2 W and the central wavelength of 1563 nm, consists of an amplified spontaneous emission (ASE) source and an Erbium-Ytterbium-doped fiber amplifier (EYDFA). The pump light is coupled into the cavity through a 1570/2000 nm filter-based wavelength division multiplexer (WDM). A polarization-insensitive isolation (PI-ISO) is used to force the laser operating unidirectionally in the UR. Two in-line polarization controllers (PC1 and PC2) are, respectively, inserted into the NALM and the UR to adjust the intra-cavity polarization. The output port is served by an optical coupler (OC) with a splitting ratio of 1:9. A piece of 4.8 m long single-mode Thulium-doped fiber (TDF), with an absorption coefficient of 13 dB/m at 1550 nm, and the dispersion parameter β_2 of −0.0707 ps^2/m at 1900 nm, is used as the gain medium. A 45 m long ultra-high
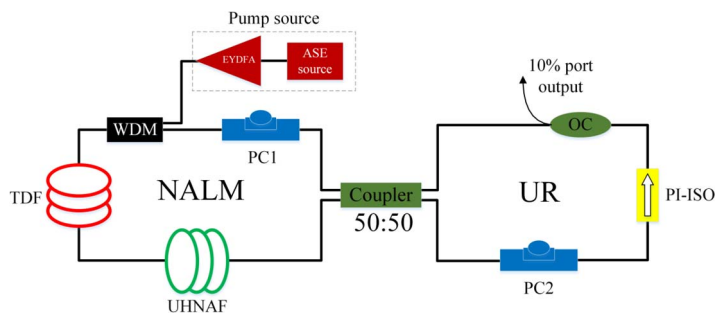
Fig. 1. Schematic of the experimental setup. WDM: wavelength division multiplexer. TDF: Thulium-doped fiber. UHNAF: ultra-high numerical aperture fiber. PC: polarization controller. PI-ISO: polarization-insensitive isolation. OC: optical coupler. NALM: nonlinear amplified loop mirror. UR: unidirectional ring.

numerical aperture fiber (UHNAF), with the core NA of 0.28 and the core diameter of 2.5 μm, is employed to compensate the cavity abnormal dispersion. Because of the small fiber core of UH-NAF, a high amount of waveguide dispersion generates and the negative material dispersion of the fiber is overcompensated. The dispersion parameter β_2 of UHNAF is estimated to be ± 0.0485 ps^2/m at 1900 nm. For stable mode-locking, the UHNAF also provides an asymmetric gain and induces enough nonlinear phase shift difference between the clockwise-propagating light and counterclockwise-propagating light in the NALM [17]. The fiber pigtails of optical components in the cavity are Corning single-mode passive fiber (SMF28) with the dispersion parameter β_2 of -0.0679 ps^2/m at 1900 nm and their length adds up to be 14.5 m. The total cavity length is about 64.3 m and the net cavity dispersion is calculated to be ± 0.8585 ps^2 at 1900 nm. The laser spectrum is measured by an optical spectrum analyzer (Yokogawa AQ6375). The pulse waveforms and the radio frequency (RF) spectrum are measured by an InGaAs photodetector (EOT ET-5000, 10 GHz) connected to a digital signal analyzer (Agilent DSA90804A, 8 GHz) and an RF spectrum analyzer (Agilent N9320A, 3 GHz).

3. Experimental Results and Discussions

The experimental laser starts the continuous wave (CW) operation at the pump power of 255 mW. The self-starting mode-locked state is observed when the pump power is increased over 583 mW. Due to the pump hysteresis effect [32], the mode-locked pulse can be maintained when the pump power decreased to 330 mW. By properly adjusting the PCs, laser operating in DSR region is easily achieved. The characteristic of the fundamental mode-locked pulses is illustrated in Fig. 2. Fig. 2(a) shows the single rectangular pulse with pulse width of 1.39 ns, and the inset shows the pulse train in 2 μs scale with cavity round trip time of 321.28 ns, which is determined by the 64.3 m cavity length. Fig. 2(b) shows the optical spectrum of the DSR laser with 0.02 nm resolution. The center wavelength locates at 1941.08 nm and the full width at half maximum (FWHM) is about 0.705 nm. No Kelly sidebands can be observed in the spectrum. The upper portion of the spectrum is a triangle-like peak with narrow width and the bottom is a wide steep-sided pedestal. It has a good match to the simulation of DSR laser operating in a normal dispersion cavity [18]. According to the above data, the time bandwidth product (TBP) is calculated to be 78.1, confirming that the pulse is heavily chirped. The RF spectrum with 10 Hz resolution is shown in Fig. 2(c). The fundamental repetition rate is 3.11 MHz. The signal-noise ratio (SNR) is about 52.7 dB, indicating that the laser operates with very low-intensity noise. The inset of Fig. 2(c) presents the RF spectrum with a scanning range of 500 MHz.

Fig. 3 shows the waveforms (a) and spectra (b) evolution of mode-locked pulses with the increasing pump power. When the pump power increases from 330 mW to 1980 mW, the pulse width varies from 480 ps to 6.19 ns continuously. The broadening behavior starts from the tail of each pulse and the profile of pulses transforms from bell-shaped form to rectangle [33]. During
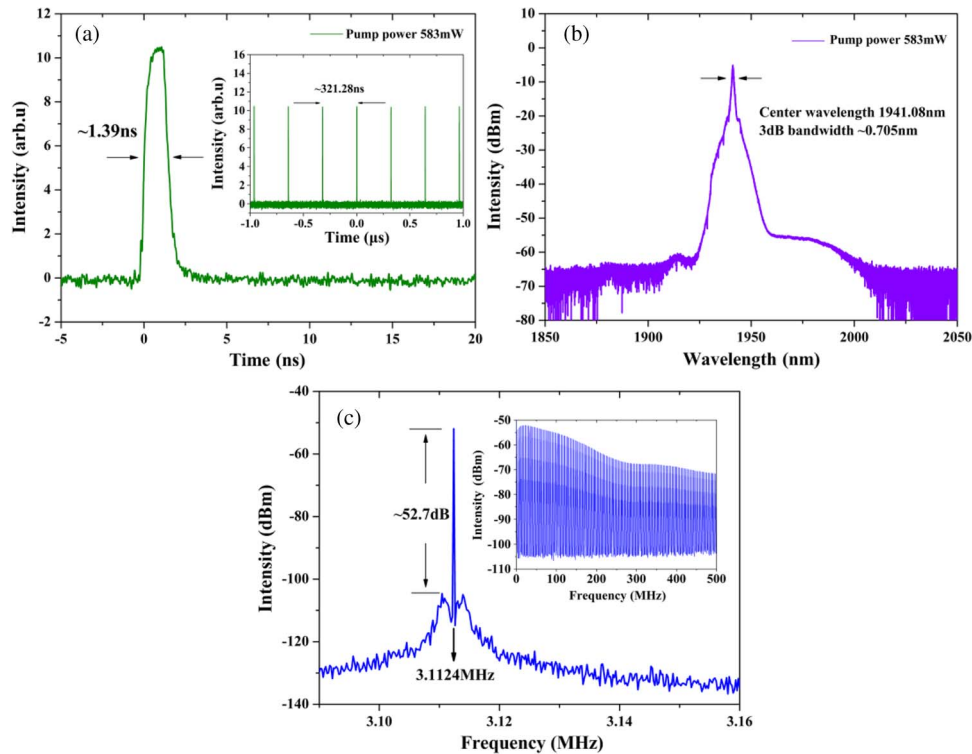
Fig. 2. Fundamental mode-locking. (a) Rectangular pulse at the pump power of 583 mW. (Inset) Pulse train. (b) Corresponding optical spectrum. (c) RF spectrum around the fundamental repetition rate. (Inset) RF spectrum with 500 MHz span.
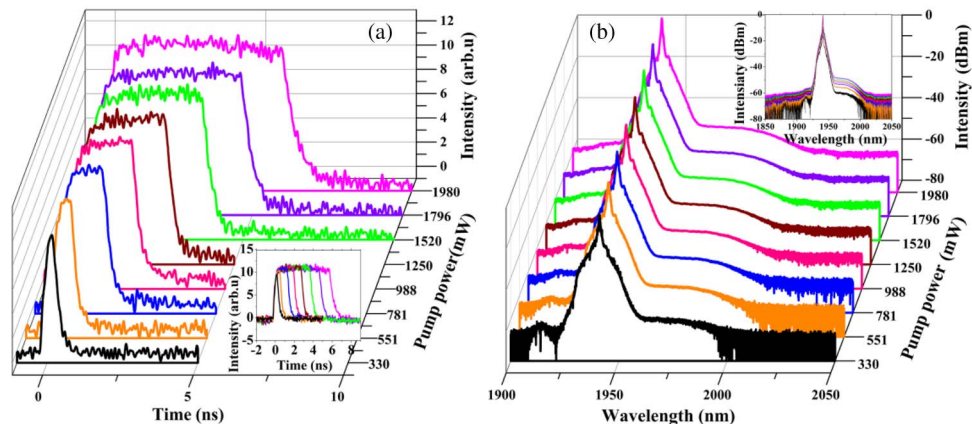

Fig. 3. (a) Evolution of rectangular pulses with increasing pump power. (b) Corresponding optical spectra.

the broadening process, the experimental laser remains single-pulse operation, no multi-pulse operating and wave-breaking can be observed. The inset of Fig. 3(a) shows that the rectangular pulse always keeps a constant amplitude though the pump power varies in a large range. Theoretically, under a high enough pump power condition, the rectangular pulse is able to further broaden, limitlessly. The above observation also well proves that the cavity parameters have satisfied the DSR condition and stable DSR laser output can be achieved in the net-normal
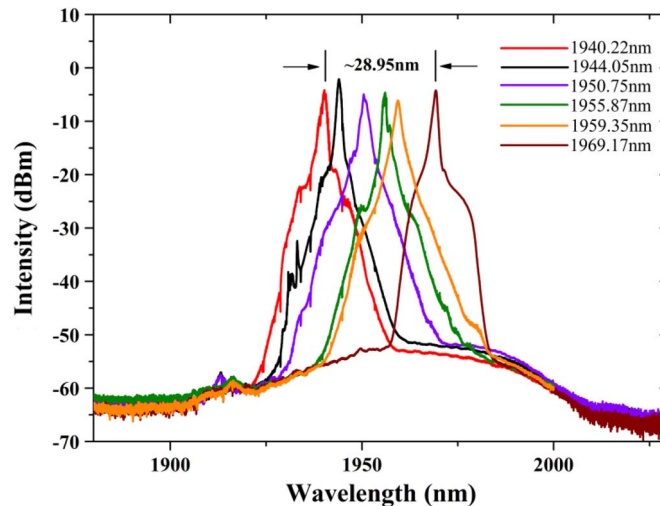
Fig. 4. Different operating wavelength of the DSR laser from 1940.22 nm to 1969.17 nm.

dispersion figure-eight TDFL. Fig. 3(b) shows the optical spectra of the DSR laser at different pump power. The spectra hold the same profile, the center wavelength and FWHM are almost in-variable with the increasing pump power. As presented in the inset of Fig. 3(b), only a slight in-crease of spectral intensity can be observed.

Moreover, we also find that the DSR laser can operate in different wavelengths. Without em-ploying any tunable wavelength-selected filter in the cavity, the DSR lasing wavelength can be tuned from 1940.22 nm to 1969.17 nm by simply adjusting the orientations of PCs. The DSR laser has a wide tunable range of about 28.95 nm. As shown in Fig. 4, under different settings of PCs, we obtain that the center wavelength of the DSR laser locates at 1940.22 nm, 1944.05 nm, 1950.75 nm, 1955.87 nm, 1959.35 nm, and 1969.17 nm, respectively. The differ-ence of the spectral intensity is caused by the different intra-cavity polarization state according to the mode-locked mechanism of the NALM technology. The wavelength-selected phenomenon can be explained by the birefringence-induced filtering effect. Each fiber bending in cavity can introduce more or less birefringence which will lead to a relative phase difference between the beams propagating along the slow and fast axes [34]. The 45 m UHNAF (and the TDF and SMF28), which is coiled into many turns, generates a large number of birefringence. Similar to a fiber-based Lyot filter [35], over a long section of coiling fiber, the accumulated phase difference is given by $\Delta\varphi = (2\pi/\lambda)L\Delta n$, where L is the length of the coiling fiber, λ is the central wave-length, $\Delta n = n_{slow} - n_{fast}$ is the strength of birefringence. In consideration of the nonuniformity of fiber bending, Δn is an average value. The transmission distribution with respect to the wavelength is a function of $\Delta\varphi$ [36]. The spectral components corresponded to the transmis-sion peak have the least loss. The transmission peak wavelength can be shifted by changing the intra-cavity polarization state. Thus, by adjusting the PCs, it is easy to realize the wave-length tuning.

In order to understand the characteristics of the DSR laser, the functional relationship graph has been plotted in Fig. 5. Pulse width, average output power, and pulse energy are all mono-tonically increasing with the pump power. At the maximum pump power of 1980 mW, the aver-age output power reaches 60.73 mW and the pulse energy is calculated to be 19.51 nJ, the OC in the UR separates about 10% of the intra-cavity power and the intra-cavity average power is approximately 607.3 mW, therefore the intra-cavity "optical to optical" efficiency is about 30.67%. The maximum pulse width is 6.19 ns and the corresponding peak power of the rectangular pulses is calculated to be 3.183 W. Due to the linear increase of pulse width and pulse energy, the peak power is clamped in a nearly constant value and the average peak power of the rectangular pulses is about 3.16 W.
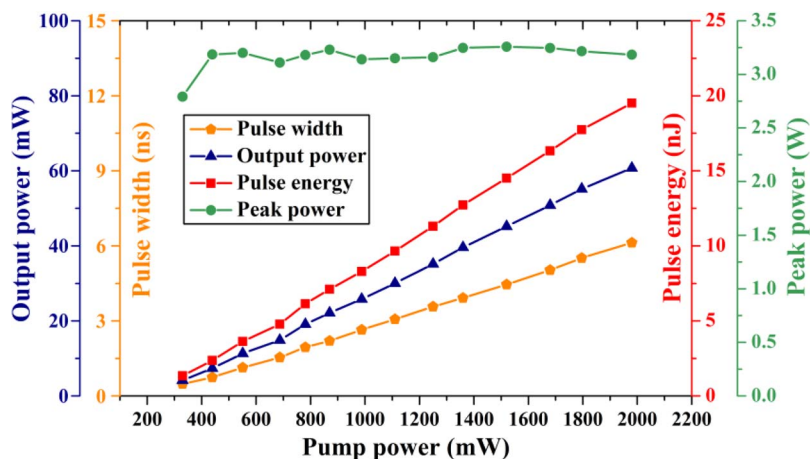
Fig. 5. Pulse width, average output power, pulse energy, and peak power versus pump power.

4. Conclusion

In conclusion, we report on an all-fiber figure-eight mode-locked TDFL. A 45 meters long UHNAF is used to manage the cavity dispersion. The net cavity dispersion parameter is calculated to be 0.8585 ps^2 at 1900 nm. Under a proper PCs setting, the experimental laser starts the operation in DSR region and generates stable rectangular pulses with a repletion rate of 3.11 MHz and maximum average output power of 60.73 mW. With increasing pump power, the rectangular pulse width can be tuned from 480 ps to 6.19 ns. The maximum pulse energy and the clamped peak power are calculated to be 19.51 nJ and 3.16 W, respectively. In addition, the birefringence imposes additional wavelength-dependent modulation, by properly adjusting the PCs, the laser can operate in a wide wavelength-tuning range of 28.95 nm, from 1940.22 nm to 1969.17 nm. The stable high-energy rectangular pulses generated from the DSR TDFL can be served as an ideal seed source in a multistage amplified laser system. It also has great potential in various application fields.

Acknowledgement

References

[1] Q. Wang, J. Geng, T. Luo, and S. Jiang, "Mode-locked 2 μm laser with highly thulium-doped silicate fiber," *Opt. Lett.*, vol. 34, no. 23, pp. 3616–3618, 2009.

[2] M. A. Solodyankin *et al.,* "Mode-locked 1.93 μm thulium fiber laser with a carbon nanotube absorber," *Opt. Lett.*, vol. 33, no. 12, pp. 1336–1338, Jun. 2008.

[3] M. Zhang *et al.,* "Tm-doped fiber laser mode-locked by graphene–polymer composite," *Opt. Exp.*, vol. 20, no. 22, pp. 25077–25084, 2012.

[4] H. Zhang, D. Y. Tang, L. M. Zhao, Q. L. Bao, and K. P. Loh, "Large energy mode locking of an erbium-doped fiber laser with atomic layer graphene," *Opt. Exp.*, vol. 17, no. 20, pp. 17630–17635, Sep. 2009.

[5] S. Huang *et al.,* "Tunable and switchable multi-wavelength dissipative soliton generation in a graphene oxide mode-locked Yb-doped fiber laser," *Opt. Exp.*, vol. 22, no. 10, pp. 11417–11426, May 2014.

[6] P. Yan *et al.,* "Microfiber-based WS2-film saturable absorber for ultra-fast photonics," *Opt. Exp.*, vol. 5, no. 3, pp. 479–489, Mar. 2015.

[7] H. Zhang *et al.,* "Molybdenum disulfide (MoS2) as a broadband saturable absorber for ultra-fast photonics," *Opt. Exp.*, vol. 22, no. 6, pp. 7249–7260, Mar. 2014.

[8] H. Liu *et al.,* "Femtosecond pulse erbium-doped fiber laser by a few-layer MoS2 saturable absorber," *Opt. Lett.*, vol. 39, no. 15, pp. 4591–4594, Aug. 2014.

[9] J. Du *et al.,* "Ytterbium-doped fiber laser passively mode locked by few-layer molybdenum disulfide (MoS2) saturable absorber functioned with evanescent field interaction," *Sci. Rep.*, vol. 4, no. 6346, Sep. 2014.

[10] C. Zhao *et al.,* "Wavelength-tunable picosecond soliton fiber laser with topological insulator: Bi_2Se_3 as a mode locker," *Opt. Exp.,* vol. 20, no. 25, pp. 27888–27895, Dec. 2012.

[11] H. Lu *et al.,* "Third order nonlinear optical property of Bi_2Se_3," *Opt. Exp.,* vol. 21, no. 2, pp. 2072–2082, Jan. 2013.

[12] H. Liu *et al.,* "Femtosecond pulse generation from a topological insulator mode-locked fiber laser," *Opt. Exp.,* vol. 22, no. 6, pp. 6868–6873, Mar. 2014.

[13] P. Yan, R. Lin, S. Ruan, A. Liu, and H. Chen, "A 2.95 GHz, femtosecond passive harmonic mode-locked fiber laser based on evanescent field interaction with topological insulator film," *Opt. Exp.,* vol. 23, no. 1, pp. 154–164, Jan. 2015.

[14] Z.-C. Luo *et al.,* "2 GHz passively harmonic mode-locked fiber laser by a microfiber-based topological insulator saturable absorber," *Opt. Exp.,* vol. 38, no. 24, pp. 5212–5215, Dec. 2013.

[15] P. Yan *et al.,* "Topological insulator solution filled in photonic crystal fiber for passive mode-locked fiber laser," *IEEE Photon. Technol. Lett.,* vol. 27, no. 3, pp. 264–267, Feb. 2015.

[16] L. E. Nelson, E. P. Ippen, and H. A. Haus, "Noiselike pulses with a broadband spectrum generated from an erbium-doped fiber laser," *Appl. Phys. Lett.,* vol. 67, no. 19, pp. 19–21, Jun. 1995.

[17] M. E. Fermann, F. Haberl, M. Hofer, and H. Hochreiter, "Nonlinear amplifying loop mirror," *Opt. Lett.,* vol. 15, no. 13, pp. 752–754, Jul. 1990.

[18] W. Chang, A. Ankiewicz, J. M. Soto-Crespo, and N. Akhmediev, "Dissipative soliton resonances in laser models with parameter management," *J. Opt. Soc. Amer. B.,* vol. 25, no. 12, pp. 1972–1977, Dec. 2008.

[19] W. Chang, J. M. Soto-Crespo, A. Ankiewicz, and N. Akhmediev, "Dissipative soliton resonances in the anomalous dispersion regime," *Phys. Rev. A.,* vol. 79, Mar. 2009, Art. ID. 033840.

[20] W. H. Renninger, A. Chong, and F. W. Wise, "Dissipative solitons in normal-dispersion fiber lasers," *Phys. Rev. A.,* vol. 77, Feb. 2008, Art. ID. 023814.

[21] W. Chang, A. Ankiewicz, J. M. Soto-Crespo, and N. Akhmediev, "Dissipative soliton resonances," *Phys. Rev. A.,* vol. 78, Aug. 2008, Art. ID. 023830.

[22] X. Wu, D. Y. Tang, H. Zhang, and L. M. Zhao, "Dissipative soliton resonance in an all-normal-dispersion erbium-doped fiber laser," *Opt. Exp.,* vol. 17, no. 7, pp. 5580–5584, Mar. 2009.

[23] L. Duan, X. Liu, D. Mao, L. Wang, and G. Wang, "Experimental observation of dissipative soliton resonance in an anomalous-dispersion fiber laser," *Opt. Exp.,* vol. 20, no. 1, pp. 266–270, Jan. 2011.

[24] S.-K. Wang *et al.,* "Dissipative soliton resonance in a passively mode-locked figure-eight fiber laser," *Opt. Exp.,* vol. 21, no. 2, pp. 2402–2407, Jan. 2013.

[25] L. Liu *et al.,* "Wave-breaking-free pulse in an all-fiber normal-dispersion Yb-doped fiber laser under dissipative soliton resonance condition," *Opt. Exp.,* vol. 21, no. 22, pp. 27087–27092, Nov. 2013.

[26] J. Yang *et al.,* "Observation of dissipative soliton resonance in a net-normal dispersion figure-of-eight fiber laser," *IEEE. Photon. J.,* vol. 5, no. 3, Jun. 2013, Art. ID. 1500806.

[27] H. Lin, C. Guo, S. Ruan, and J. Yang, "Dissipative soliton resonance in an all-normal-dispersion Yb-doped figure-eight fire laser with tunable output," *Laser Phys. Lett.,* vol. 11, 2014, Art. ID. 085105.

[28] X. Li *et al.,* "Highly efficient rectangular pulse emission in a mode-locked fiber laser," *IEEE. Photon. Technol. Lett.,* vol. 26, no. 20, pp. 2082–2085, Oct. 2014.

[29] R. Gumenyuk, I. Vartiainen, H. Tuovinen, and O. G. Okhotnikov, "Dissipative dispersion-managed soliton 2 μm thulium/holmium fiber laser," *Opt. Lett.,* vol. 36, no. 5, pp. 609–611, 2011.

[30] F. Haxsen, D. Wandt, U. Morgner, J. Neumann, and D. Kracht, "Monotonically chirped pulse evolution in an ultrashort pulse thulium-doped fiber laser," *Opt. Lett.,* vol. 37, no. 6, pp. 1014–1016, Mar. 2012.

[31] A. Wienke *et al.,* "Ultrafast, stretched-pulse thulium-doped fiber laser with a fiber-based dispersion management," *Opt. Lett.,* vol. 37, no. 13, pp. 2466–2468, Jul. 2012.

[32] A. Komarov, H. Leblond, and F. Sanchez, "Multistability and hysteresis phenomena in passively mode-locked fiber lasers," *Phys. Rev. A.,* vol. 71, May 2005, Art. ID. 053809.

[33] A. Komarov, F. Amrani, A. Dmitriev, K. Komarov, and F. Sanchez, "Competition and coexistence of ultrashort pulses in passive mode-locked lasers under dissipative soliton resonance conditions," *Phys. Rev. A.,* vol. 87, Feb. 2013, Art. ID. 023838.

[34] S. J. Garth, "Birefringence in bent single-mode fibers," *J. Lightw. Technol.,* vol. 6, no. 3, pp. 445–449, Jun. 1988.

[35] G. Shabtay and E. Eidinger, "Tunable birefringent filters—Optimal iterative design," *Opt. Exp.,* vol. 10, no. 26, pp. 1534–1541, Dec. 2002.

[36] K. Özgören and F. Ö. Ilday, "All-fiber all-normal dispersion laser with a fiber-based Lyot filter," *Opt. Lett.,* vol. 35, no. 8, pp. 1296–1298, Apr. 2010.